We are IntechOpen, the world's leading publisher of Open Access books Built by scientists, for scientists

4,800
Open access books available

122,000
International authors and editors

135M
Downloads

Our authors are among the

154
Countries delivered to

TOP 1%
most cited scientists

12.2%
Contributors from top 500 universities

CLARIVATE ANALYTICS BOOK CITATION INDEX INDEXED

WEB OF SCIENCE™

Selection of our books indexed in the Book Citation Index in Web of Science™ Core Collection (BKCI)

Interested in publishing with us?
Contact book.department@intechopen.com

Numbers displayed above are based on latest data collected.
For more information visit www.intechopen.com

21

Performance Evaluation of Single-Channel Receivers for Wireless Optical Communications by Numerical Simulations

M. Castillo-Vázquez, A. Jurado-Navas, J.M. Garrido-Balsells
and A. Puerta-Notario
Communications Engineering Department, University of Málaga
Campus de Teatinos, Málaga
Spain

1. Introduction

In the last decade, the growing demand of high-speed portable computer terminals in office environment is promoting the development of broadband wireless local area networks (WLAN). Within this field, wireless infrared communications represent a viable alternative to radio frequency for short-range indoor transmission, with many significant advantages such as enormous potential bandwidth, security and low component price (Kahn & Barry, 1997). However, system design for indoor WLAN is conditioned by the especially harmful characteristics of the optical channel, i.e. high attenuation, elevated ambient light noise and multipath distortion (Kahn et al., 1994). These inconveniences make infrared systems demand high levels of optical power to achieve a sufficient signal-to-noise ratio (SNR), and limit high-speed performance.

To mitigate such inconveniences, a wide choice of transmitters and receivers designs have been proposed so far (Alves et al., 2000; Bellon et al., 1999; Carruther & Kahn, 2000; Jivkova & Kavehrad, 2001; Jungnickel et al., 2003; Yun & Kavehrad, 1992). Among all, the combined use of multibeam transmitters and angle diversity receivers has become the preferred solution in the literature (Carruther & Kahn, 2000; Djahani & Kahn, 2000; Jivkova & Kavehrad, 2001). In this configuration, the multibeam transmitter (MBT) is used to distribute the optical power within the room, creating a regular lattice of spots on the ceiling where the light is concentrated. Signals from these spots are collected by the multiple optical elements of conventional angle diversity receivers (ADR) and properly combined in order to increase the overall SNR.

There are two main ways to implement an angle diversity receiver. In the conventional approach, the receiver consists of various branches which are oriented in different directions. Each branch comprises a separate nonimaging concentrator and a small photodetector. Since each concentrator only receives signals from a small region of the room, the conventional angle diversity receiver can reduce ambient light noise and multipath distortion by tuning the weights of each branch. The second structure, referred to as imaging angle diversity receiver, consists of a single imaging optical concentrator (e.g., a lens) that forms an image of

the received light on a segmented array of photodetectors (pixels) placed at its focal plane. This receiver has two major advantages over nonimaging angle-diversity receivers. First, all photodetectors share a common concentrator, thus reducing size and cost. Second, all photodetectors can be laid out in a single planar array, enabling the use of a large number of receiving elements or pixels. The use of multibeam transmitters in conjunction with angle diversity receivers (imaging and non-imaging) improves channel bandwidth and received SNR (Carruther & Kahn, 2000; Kahn et al., 1998; Tang et al., 1996).

However, in spite of the advantages of the above mentioned structures, the performance of wireless optical links can be further improved. In this sense, two novel receiver designs, alternative to angle diversity receivers, were proposed by the authors in (Castillo-Vázquez et al., 2004) and (Castillo-Vázquez & Puerta-Notario, 2005), respectively. These new receivers, known as single-channel receivers (SCR), share the same design idea, which is to provide their single optical front-end with self-orienting capability. Thus, they can automatically aim at the optimum ceiling area in terms of illumination. The self-orienting capability of both SCR, together with the very narrow field of view (FOV) employed, drastically reduces path loss, background noise and multipath distortion. Moreover, its single-channel structure minimizes hardware complexity to a minimum and, consequently, also reduces power consumption, compared to ADR which use multiple channels.

In this chapter, the work presented in (Castillo-Vázquez et al., 2004) and (Castillo-Vázquez & Puerta-Notario, 2005) is extended to investigate the impact of both SCR on channel characteristics. By numerical simulations, the main performance indicators of two link configurations, formed by a MBT and the proposed SCR, are obtained. These link simulations are used to analyze the effect of diverse design aspects in the system performance. In particular, two points are investigated (a) the effect of transmitter spots size and ambient light sources (natural and artificial) on SNR and channel bandwidth (BW), and (b) the impact of the receivers total FOV and blockage on the transmitter power requirements. The results obtained in these simulations show the robustness and weaknesses of each receiver structure and prove the great potential of both SCR when operating in a multispot diffusing configuration. The chapter is organized as follows. The second section is focused on the characteristics and structure of single-channel receivers. In the third section, the transmitter and ambient light models employed in the numerical analysis are presented. In section four, the performance evaluation of receivers is carried out. Conclusions are presented in the last section.

2. Single-channel receivers

Fig. 1 depicts the structure of the two single-channel receivers under study. Both receivers use an optical concentrator to increase the received optical signal power, and an optical bandpass filter to reject ambient light. For the sake of clarity, this filter is not shown in the figure.

As shown in Fig. 1 (a), a conventional single-channel receiver (CSCR) consists of an objective lens-photodetector set mounted on an electromechanical orienting system that moves the optical front-end in azimuth ϕ_r and elevation θ_r angles. In this structure, a SNR estimator and a maximum search algorithm are used to automatically aim the receiver at the room area with higher SNR. A CSCR, thus, is able to point to the best ceiling spot, avoiding the areas with strong ambient light. This is based on the fact that this light is normally received from a different direction than the desired signal, as shown in Fig. 1 (a). Thus, this receiver can completely reject the light from artificial lamps if they are placed far from the selected

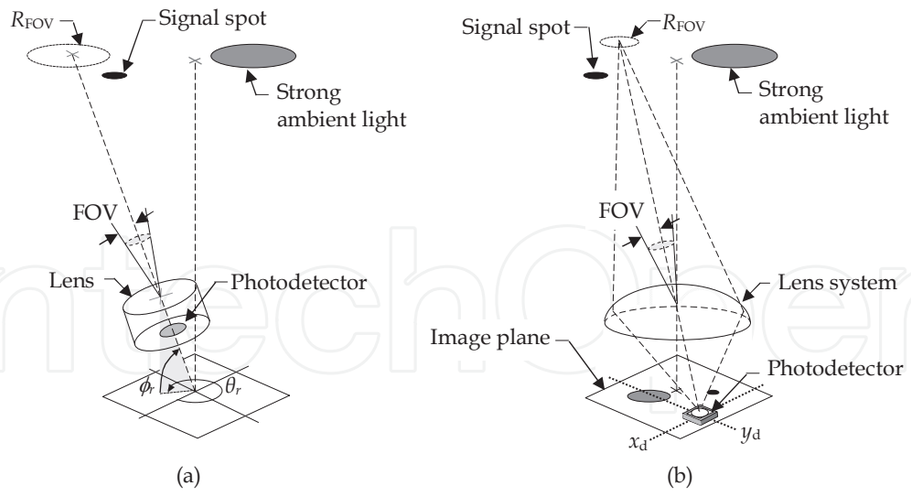

Fig. 1. (a) Conventional single-channel receiver (CSCR). (b) Single-channel imaging receiver (SCIR). The CSCR employs a lens in conjunction with a single photodetector. The SCIR employs an imaging lens system combined with a small photodetector placed on a miniaturized positioning mechanism.

spot. In addition, the receiver can work with an extremely narrow FOV, since it is pointed to the optimum direction, which allows the use of a positive lens as optical concentrator with high gain and, consequently, reducing the detector dimensions. Note that this reduction is in accordance with the purpose of attaining high bit rates. The FOV value optimizing signal and noise levels in the receiver can be obtained geometrically as

$$\mathrm{FOV} = \tan^{-1}(D_{\mathrm{spot}}/2h), \tag{1}$$

where D_{spot} is the diameter of the ceiling spots and h is the distance between receiver and ceiling. Since in many office rooms the receivers are placed at a desktop level (about 90 cm above the floor), it can be assumed that the distance h is approximately 2 m. Moreover, as will be explained later, a spot diameter D_{spot}=10 cm is considered as a reasonable size for our system. Thus, Eq. (1) yields to a receiver FOV of approximately 1.5°. To obtain this FOV, the CSCR uses a positive lens with a 2-cm diameter and an f-number ($f/\#$) of 2 (i.e., $f/2$), in conjunction with a circle photodetector of diameter

$$D_{\mathrm{det}} = 2D\mathrm{f}/\#\tan(\mathrm{FOV}). \tag{2}$$

Hence, a $D_{\mathrm{det}} = 2$ mm is needed to achieve the required FOV. Another important parameter of a CSCR is the total field of view ($\mathrm{FOV}_{\mathrm{total}}$). Such a parameter defines the permitted range of pointing directions for the receiver front-end, depending on the constraints of the electromechanical system. Although, in practice, any value for this parameter is possible, it has been chosen a $\mathrm{FOV}_{\mathrm{total}} = 45°$ in order to keep the blockage probability under reasonable limits. Despite all, if a blockage is produced, receiver must find an alternative spot. Blockage in MBT configurations is further investigated in (Jivkova & Kavehrad, 2003). Note that, with a $\mathrm{FOV}_{\mathrm{total}} = 45°$, the CSCR covers a total ceiling area of 12.5 m^2.

The second receiver structure is depicted in Fig. 1 (b). This structure, referred to as single-channel imaging receiver (SCIR), comprises an imaging lens system combined with a

small photodetector placed on a miniaturized positioning mechanism. Here, the positioning system allows the photodetector to move along the X-Y axes defining the focal plane of the lens system. With such a structure, the receiver can modify its orientation, determined by the elevation and azimuthal angles (θ_r, ϕ_r), changing the photodetector coordinates (x_d, y_d). In a SCIR, the photodetector size defines the receiver FOV and, consequently, the dimensions of the ceiling region R_{FOV}, as shown in Fig. 1 (b). Unlike CSCR, the optical concentrator here is not a simple lens, but a system consisting of several lenses acting as an imaging concentrator. Thus, it images part of the room ceiling onto the receiver image plane. Such an image contains areas with signal light (spot images) and areas with ambient light, as shown in Fig. 1 (b). In our design, a SNR estimator and a maximum search algorithm are used to move the photodetector to the coordinates with better SNR. Note that these coordinates usually coincide with the position of the spot image closest to the receiver. Moreover, since spot images are minute, the receiver can used a very small photodetector to detect them, thus ensuring an optimal ratio between collected signal and noise levels. In a SCIR, the size of the photodetector is chosen equal to the size of spot images. Therefore, its diameter is given by

$$D_{\text{det}} = |M_T| \, D_{\text{spot}}, \tag{3}$$

where M_T is the magnification of the lens system, obtained from the distance to the image plane d_{img} and h as $M_T = -d_{img}/h$. Note that, in this design, d_{img} is approximately the focal length.

To achieve a large total FOV at a low level of optical aberrations, while maintaining a reasonable size of the image plane, a lens system similar to the designs proposed in (Djahani & Kahn, 2000) and (Jivkova et al., 2004), is used. In particular, the lens system used has an aperture diameter of 3 cm and $f/1$. This large aperture is needed to ensure an acceptable signal power in the photodetector. Likewise, to obtain a good image quality and avoid shifting problems in the optical interference filter (Kahn & Barry, 1997), the receiver total FOV is limited to 30°. In these conditions, the distance from the lens system to the image plane is d_{img}=3.05 cm, and the image plane diameter is 35 mm. Assuming, again, a spot diameter D_{spot}=10 cm, Eq. (3) yields to D_{det}= 1.52 mm. With a $\text{FOV}_{\text{total}} = 30°$, the resulting SCIR covers a total ceiling area of approximately 4.1 m^2.

3. Signal and ambient light modeling

In this section, we describe the model of the multibeam transmitter and the model of the light noise sources used in our numerical analysis. Together with this description, the expressions for the signal and light power received on both single-channel receivers, are also deduced. These expressions will be used in section 4 to analyze system performance.

3.1 Multibeam transmitter

As mentioned in the introduction, a multibeam transmitter is formed by multiple narrow beams pointing in different directions towards the ceiling room. These narrow beams project onto the ceiling a spot pattern that can adopt very diverse geometries. In the literature, a great variety of geometries have been proposed so far. These geometries include uniform patterns, in which the spots are organized in regular lattices as those in (Jivkova & Kavehrad, 2005; 2000) and non-uniform patterns, in which the spots are arranged in a more elaborated

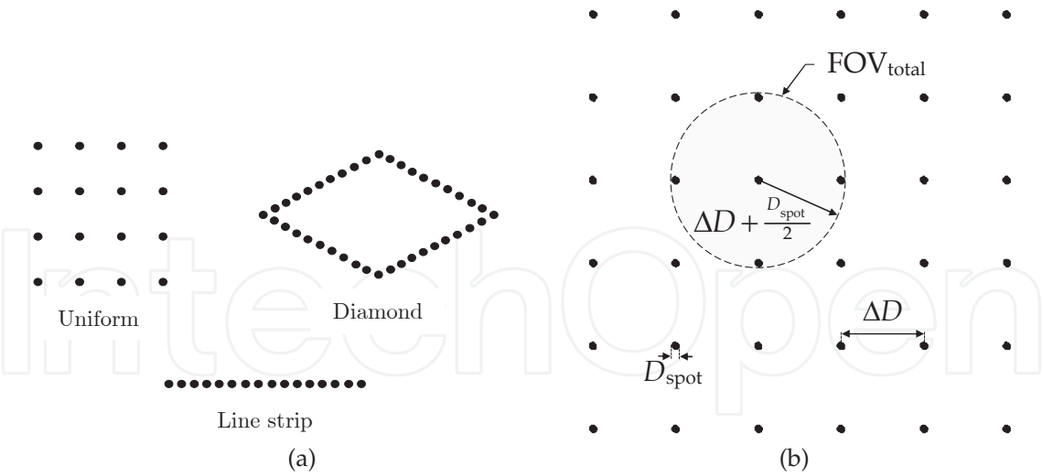

Fig. 2. (a) Transmitter pattern geometries proposed in the literature. (b) Transmitter pattern used in our analysis.

way, forming a strip line as in (Al-Ghamdi & Elmirghani, 2004a) or a diamond shape as in (Al-Ghamdi & Elmirghani, 2004b). Some examples of these geometries are shown in Fig. 2 (a). Although line strip and diamond transmitters offer some advantages when used in combination with pyramidal receivers (Al-Ghamdi & Elmirghani, 2003a;b; 2004a), in our case, uniform patterns are best suited to the operation of single channel receivers. Therefore, for this analysis, we have chosen a uniform transmitter that creates a square mesh pattern on the ceiling as the one depicted in Fig. 2 (b). This pattern is formed by M circular spots of diameter D_{spot} with a spot grid spacing ΔD. In practice, this transmitter can be implemented by using a single laser source together with a holographic or diffractive optical element, as described in (Eardley et al., 1996; Kavehrad & Jivkova, 2003; Pakravan et al., 1996). The choice of ΔD, M and D_{spot} greatly affects system performance. Here, some criteria to choose these parameters are described.

In order to provide immunity against blockage, the transmitter pattern is designed so that at least two signal spots lie within the receiver total FOV. Thus, if the selected spot is obstructed, receivers can point to a different one to avoid a link failure. To fulfill this condition, the grid spacing ΔD must satisfy that $h \tan(\text{FOV}_{\text{total}}) \geq \Delta D + D_{\text{spot}}/2$, as deduced from the geometry of Fig. 2 (b). Thus, from this relation, the condition becomes

$$\Delta D \leq h \tan(\text{FOV}_{\text{total}}) - \frac{D_{\text{spot}}}{2}. \tag{4}$$

According to this expression, a CSCR (with a $\text{FOV}_{\text{total}} = 45°$) would require a transmitter with higher grid spacing ΔD than a SCIR (with a $\text{FOV}_{\text{total}} = 30°$), and, as a consequence, for the same room dimensions, the MBT employed with CSCR would need fewer signal spots than the MBT of a SCIR. For instance, if we assume a rectangular room of X m $\times$ Y m, the minimum number of spots required to provide immunity against blockage is given by

$$M = (\lfloor X/\Delta D \rfloor + 1)(\lfloor Y/\Delta D \rfloor + 1) \tag{5}$$

where $\lfloor\rfloor$ represents the floor function, and ΔD is the maximum grid spacing satisfying Eq. (4).

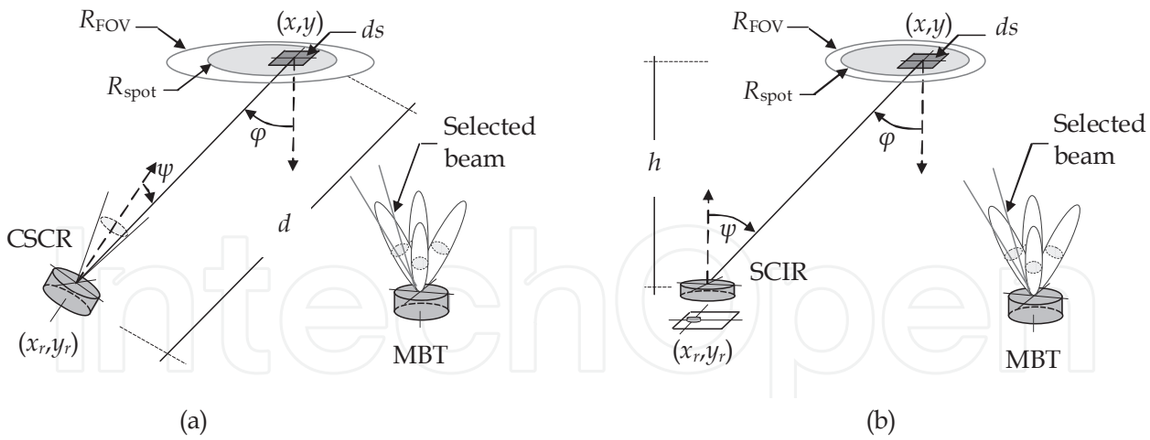

Fig. 3. (a) Link geometry used to compute the received power signal in a conventional single-channel receiver. (b) Link geometry used to compute the received power signal in a single-channel imaging receiver.

After choosing ΔD and M, the last parameter of the considered MBT is the spot diameter D_{spot}. This is the most important parameter, since it affects simultaneously several aspects of system performance. Note that, whenever the spot size is reduced, the SNR and the channel BW are significantly improved. Our results show that channel BW doubles and SNR increases approximately by 6 dB every time the spot diameter D_{spot} is halved. However, such an improvement in SNR and BW is achieved at the expense of complicating the search process in the pointing algorithm, which needs approximately five times the time to find the optimum direction. Thus, a trade-off solution must be found. For this purpose, different simulations in a typical room office are carried out, varying the spot diameter from 5 to 20 cm in steps of 5 cm. Based on the results of these simulations, it is concluded that a spot diameter of 10 cm is needed to achieve a channel BW higher that 1 GHz with a reasonable search time.
In our analysis, the considered MBT emits a total average power P_{tx}, which is equally divided among M beams. The value of M depends on the type of receiver employed (a CSCR or a SCIR), as deduced from Eq. (4) and Eq. (5). Due to the highly collimated nature of beams emerging from the transmitter, the path loss between the transmitter and the ceiling is neglected in our simulations. Thus, all transmitter power is assumed to be concentrated within M small ceiling spots with a diameter $D_{\text{spot}} = 10$ cm. Among these spots, only one (the best) is selected by single-channel receivers and, hence, only one is used in the calculations. To compute the received power from this spot, the covered region of the ceiling, R_{spot}, is divided into differential surface elements ds, as shown in Fig. 3. Then, as in (Carruther & Kahn, 2000), theses elements are modeled as first order Lambertian emitters with a transmit power per steradian given by

$$I_{\text{spot}}(\varphi) = \frac{4\rho P_{tx} ds}{\pi^2 M D_{\text{spot}}} \cos(\varphi), \tag{6}$$

where ρ represents the ceiling reflectivity and φ is the emission angle relative to the normal. It is worth noting here that the assumption that the ceiling behaves as a diffuse reflector (i.e., a Lambertian emitter) is only valid for angles of incidence below 65°, since for higher angles, especially above 70°, the ceiling reflections exhibit a strong specular component, as described in (Gfeller & Bapst, 1979). This condition limits the maximum size of a room illuminated by a single transmitter. For instance, assuming a distance between the transmitter and the ceiling

$h_t = 2$ m, the maximum room diagonal is given by $2h_t \tan(65^\circ) = 8.6$ m (Jivkova & Kavehrad, 2001). Therefore, a square room of 6 m $\times$ 6 m would fulfill this condition.
According to the geometry of Fig. 3, the average power reflected by a ceiling element ds and detected by a SCR can be written as

$$dP_r = \frac{4\rho P_{tx} ds}{\pi^2 M D_{\text{spot}}^2} \cos(\varphi) \cdot \frac{A \cos(\psi)}{d^2}, \tag{7}$$

where A is the receiver entrance area, ψ is the angle between the surface normal to the receiver and the incident ray, and d is the distance between the transmitter and the surface element ds. Here, the value of $\cos(\varphi)$ is h/d, and the distance d can be written as a function of h, the reflector coordinates (x, y) and the receiver position (x_r, y_r) as

$$d = \sqrt{(x - x_r)^2 + (y - y_r)^2 + h^2}. \tag{8}$$

Note that the only difference between the two single-channel receivers when calculating dP_r is the value of the angle ψ. For the CSCR, this angle depends on the receiver orientation (θ_r, ϕ_r), and can be geometrically obtained from Fig. 3 (a) as

$$\psi = \cos^{-1}\left(\frac{(x - x_r)\cos(\varphi_r)\cos(\theta_r) + (y - y_r)\sin(\varphi_r)\cos(\theta_r) + h\sin(\theta_r)}{d}\right). \tag{9}$$

On the other hand, in the case of the SCIR, ψ equals ϕ and, therefore, $\psi = \cos^{-1}(h/d)$, as deduced from Fig. 3 (b).
The total reflected signal incident on the receivers is then computed by integrating the contributions of all surface elements ds within the region illuminated by the selected beam R_{spot}. In a CSCR, this total power is given by

$$P_{r,\text{CSCR}} = \frac{4\rho P_{tx} h A}{\pi^2 M D_{\text{spot}}^2} \int\limits_{(x,y)\in R_{\text{spot}}} \frac{\cos(\psi)\, ds}{\left[(x - x_r)^2 + (y - y_r)^2 + h^2\right]^{3/2}}, \tag{10}$$

where the value of the angle ψ is obtained from Eq. (9). Similarly, the total power for a SCIR is given by

$$P_{r,\text{SCIR}} = \frac{4\rho P_{tx} h^2 A}{\pi^2 M D_{\text{spot}}^2} \int\limits_{(x,y)\in R_{\text{spot}}} \frac{ds}{\left[(x - x_r)^2 + (y - y_r)^2 + h^2\right]^2}. \tag{11}$$

3.2 Ambient light sources

In an indoor environment, the mayor sources of ambient light include sunlight, incandescent light and fluorescent light sources (Barry, 1994; Boucouvalas, 1996; Gfeller & Bapst, 1979; Otte et al., 1999). These sources radiate a substantial amount of power within the wavelengths of silicon photodetectors, inducing shot noise in receivers (Moreira et al., 1997; Tavares et al., 1995). Shot noise is the main degrading factor in wireless optical communications. Here, the case of sunlight and incandescent illumination is considered.
Sunlight is, certainly, the strongest source of ambient light. Normally, this light illuminates rooms after being reflected on ceiling and walls. For this reason, to model sunlight, it is assumed that ceiling acts as a secondary source of radiation. The effect of walls is neglected

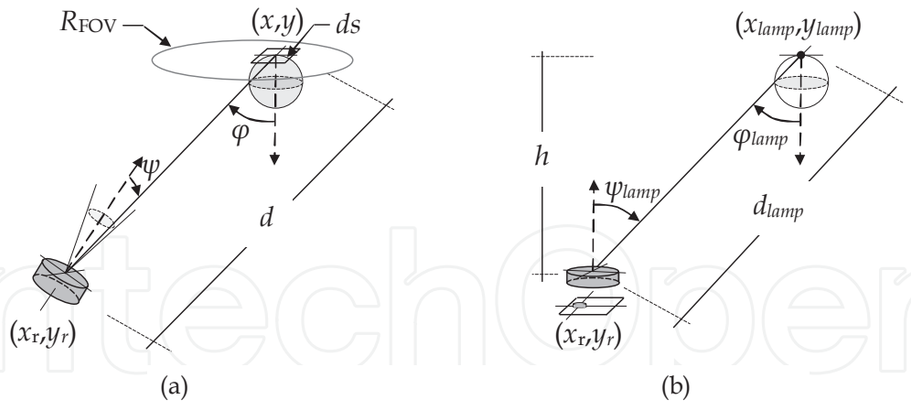

Fig. 4. (a) Link geometry used to compute the sunlight power received by a conventional single-channel receiver. (b) Link geometry employed to compute the artificial light power received by single-channel imaging receiver.

in the analysis because it does not affect single-channel receivers. As in (Carruther & Kahn, 2000), to compute the received ambient light power, the ceiling area within the receivers FOV, R_{FOV}, is divided into differential surface elements ds, acting as first order Lambertian emitters with a spectral radiant emittance given by $S_n(x,y)$. Then, according to the geometry of Fig. 4, the sunlight power detected by a single-channel receiver is obtained as

$$P_{sun} = \int_{R_{\text{FOV}}} S_n(x,y)\Delta\lambda \frac{\cos(\varphi)}{\pi} \cdot \frac{A\cos(\psi)}{d^2} \cdot ds, \tag{12}$$

where, $\Delta\lambda$ is the bandwidth of the receiver optical filter, φ is the angle between the reflected light and the normal of ds given by $\varphi = \cos^{-1}(h/d)$, ψ is the angle between the surface normal of detector and the incident ray, and d is the distance between the receiver and each differential surface element ds. Here, the differences in computing Eq. (12) between both types of receivers are two: the value of the angle ψ, and the size and geometry of the region R_{FOV}. Referring to Fig. 4 (a), the total sunlight power received in a CSCR is obtained from Eq. (12) as

$$P_{sun,\text{CSCR}} = \int_{(x,y)\in R_{\text{FOV}}} \frac{S_n\Delta\lambda(x,y)\,hA\cos(\psi)}{\pi\left[(x-x_r)^2+(y-y_r)^2+h^2\right]^{3/2}} ds, \tag{13}$$

where R_{FOV} is an ellipse whose size depends on the receiver orientation, and the angle ψ is obtained from Eq. (9). Likewise, the total natural light power for the SCIR is given by

$$P_{sun,\text{SCIR}} = \int_{(x,y)\in R_{\text{FOV}}} \frac{S_n\Delta\lambda(x,y)\,h^2A}{\pi\left[(x-x_r)^2+(y-y_r)^2+h^2\right]^{2}} ds, \tag{14}$$

where now R_{FOV} is a circle whose area depends on the receiver photodetector diameter and the lens magnification M_T. For this receiver, the angle ψ equals φ.

As previously mentioned, artificial light from incandescent lamps is much weaker than sunlight and greatly depends on the relative position of the receivers with respect to these lamps. Different measurements from ceiling lamps carried out by (Tavares et al., 1995) show that an excellent model for their radiant intensities is a generalized Lambertian pattern of

order m. Thus, in our analysis incandescent lamps are modeled as point sources with a radiant intensity given by

$$I_{\text{lamp}}\left(\varphi_{lamp}\right) = P_l \frac{m+1}{2\pi} \cos^m\left(\varphi_{lamp}\right), \tag{15}$$

where P_l represents the lamp power within the receiver optical bandwidth $\Delta\lambda$, and φ_{lamp} is the emission angle respect to the normal, as shown in Fig. 4 (b).
Referring to Fig. 4 (b) and employing the Lambertian model of Eq. (15), the received ambient light power from an incandescent lamp within the receiver FOV (of a CSCR or a SCIR) is given by

$$P_{lamp} = \frac{P_l\,(m+1)\,h^m A \cos\left(\psi_{lamp}\right)}{2\pi\left[(x_{lamp}-x_r)^2 + (y_{lamp}-y_r)^2 + h^2\right]^{\frac{m+2}{2}}} \tag{16}$$

where h is the vertical separation between the receiver and the lamp, ψ_{lamp} is the reception angle respect to the normal, and (x_{lamp}, y_{lamp}) are the ceiling lamp coordinates. Again, the only difference in computing Eq. (16) between the two types of receivers is the value of the angle ψ_{lamp}. For the CSCR, ψ_{lamp} is calculated using Eq. (9) replacing (x, y) by (x_{lamp}, y_{lamp}) and changing d by the distance between the lamp and the receiver d_{lamp}. For the SCIR, ψ_{lamp} is given by $\cos^{-1}(h/d_{lamp})$, as deduced from Fig. 4 (b).

4. Performance evaluation

In order to analyze the effect of SCR structures on system performance, two link configurations formed by a MBT and a SCR have been simulated. Both the MBT and the SCR are designed according to the criteria described in Sections 2 and 3, respectively. In these simulations, the main system performance indicators: the SNR and the channel BW, have been computed in a typical indoor environment under natural and artificial light sources. To compute the SNR, it is has been assumed that shot noise induced by ambient light is the dominant noise in the receivers. Under this assumption, the average electrical SNR in our direct-detection receivers is given by

$$\text{SNR} = \frac{(rP_r)^2}{2qrB_nP_{amb}}, \tag{17}$$

where r is the photodetector resposivity, P_r is the signal power received in the photodetector, which is obtained using Eq. (10) or Eq. (11) depending on the type of receiver considered (the CSCR or the SCIR), q is the electron charge, B_n is the receiver equivalent noise bandwidth, and P_{amb} is the received ambient light power. The value of P_{amb} is obtained adding natural and artificial light powers

$$P_{amb} = P_{sun} + P_{lamp}. \tag{18}$$

Here, P_{sun} is the ambient light power received from the sunlight, which is computed using Eq. (13) and Eq. (14) for CSCR and SCIR, respectively, and P_{lamp} is the ambient light power received from a ceiling lamp given by Eq. (16). Note that, due to the narrow FOV of SCR, these receivers only collect light from a single ceiling lamp.
On the other hand, to compute the channel BW, the impulse responses $h(t)$ of all the links are firstly obtained. To this end, it has been used a simulation tool similar to the one developed by (Barry et al., 1993), but considering only the first bounce. This simplification is possible

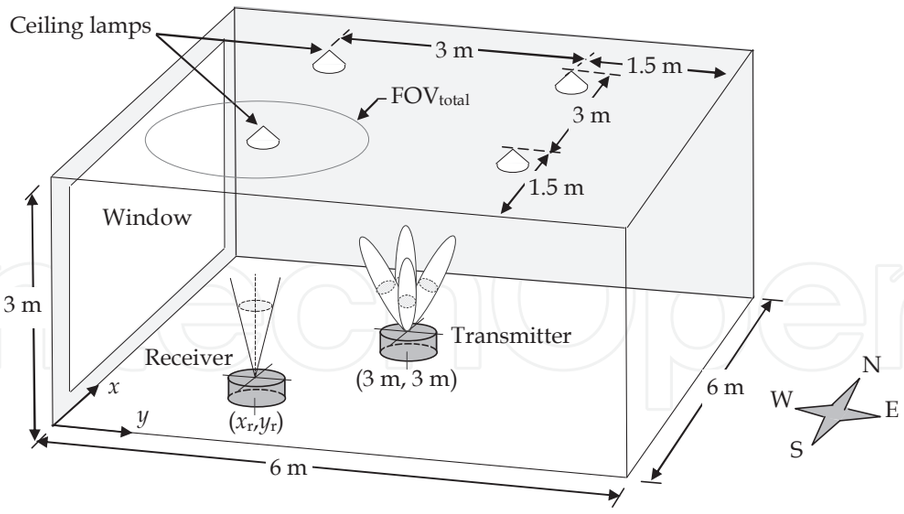

Fig. 5. Room model considered in our numerical analysis. Ambient light includes sunlight (through the window) and four incandescent lamps.

because when a MBT and a narrow FOV receiver are employed, the first bounce provides enough information on the achievable channel bandwidth, as described in (Akavan et al., 2002). Then, from $h(t)$ the frequency response is computed using $H(f) = \int_{-\infty}^{\infty} h(t)e^{-j2\pi ft}dt$, and, finally, $H(f)$ is used to determine the 3-dB channel BW (B).

4.1 Simulation set-up

Fig. 5 shows the room considered in the simulations. As can be observed, it is an empty room with dimensions 6 m $\times$ 6 m $\times$ 3 m, in which a big window occupies the west wall. The effect of the sunlight which illuminates the room through the window, is taken into account considering that the ceiling spectral emittance $S_n(x, y)$ varies linearly from 0.03 W/m^2/nm at the west edge ($y = 0$), to 0.01 W/m^2/nm at the east edge ($y = 6$). The values of S_n are taken from measurements made by Carruthers, published in (Carruther & Kahn, 2000). Four ceiling lamps have been also included in the room placed at the coordinates (x_{lamp}, y_{lamp})=(1.5, 1.5), (1.5, 4.5), (4.5, 1.5) and (4.5, 4.5), respectively, as depicted in Fig. 5. According to the explanation given in Section 3, these lamps have been modeled as Lambertian emitters of order m =2, with a power spectral density $p_{lamp} = 0.037$ W/nm within the receiver filter passband. The values of m and p_{lamp} have been taken from (Carruther & Kahn, 2000) and (Djahani & Kahn, 2000). Note that, the lamp power $P_l = p_{lamp}\Delta\lambda$. A ceiling reflectivity $\rho = 0.7$ is assumed.

In the simulations, two link configurations have been analyzed. The first configuration (CSCR links) employs a MBT and a CSCR. The second (SCIR links) uses a different MBT combined with a SCIR. In CSCR links, the receiver is composed of a lens with an aperture area $A = 3.14$ cm^2 and a photodetector with $D_{\text{det}} = 2$ mm. The resulting CSCR achieves a FOV=1.5° within a FOV$_{\text{total}} = 45°$. Together with this receiver, the considered MBT is formed by $M = 16$ circular spots with $D_{\text{spot}} = 10$ cm and a pattern grid spacing $\Delta D = 1.95$ m. On the other hand, in SCIR links, the receiver uses an imaging lens system with an aperture area $A = 7$ cm^2 and a FOV$_{\text{total}} = 30°$. In this SCIR, the circular photodetector has a diameter D_{det}= 1.52 mm. Combined with this receiver, now, the considered MBT is composed of $M = 36$ spots with a $\Delta D = 1.1$ m. The values of ΔD and M have been computed using

Eq. (4) and Eq. (5), respectively. We have also assumed that both receivers have an equivalent noise BW $B_n = 500$ MHz, an optical bandpass filter having a half-power BW $\Delta\lambda = 50$ nm and photodetectors with $r = 0.6$ A/W of resposivity. It should be pointed out here that, although particular values for r, $\Delta\lambda$, B_n and ρ are assumed in the simulations, the conclusions obtained based on the comparison of the two receivers are valid, regardless of the values employed.
In all simulated links, it is assumed that MBT are kept fixed in the center of the room at a height of 1 m, while receivers are placed in different locations. Therefore, MBT and receivers positions are given by $(3, 3)$ and (x_r, y_r), respectively, as show in Fig. 5. The distance between receivers and ceiling is $h = 2$ m.

4.2 Simulation results

Fig. 6 presents SNR and channel BW spatial distributions for the two link configurations, as function of the the receiver position within the room. To obtain these results, receiver coordinates (x_r, y_r) has been changed along the room surface with a grid spacing of 10 cm. These coordinates are given with respect to the southwest corner, as shown in Fig. 5. A transmitter power $P_{tx} = 200$ mW is assumed in all cases. In this figure, it is observed that the two SNR spatial distributions present M local maximum corresponding to the coordinates of the ceiling spots: 16 maximum for CSCR links (Fig. 6 (a)) and 36 for SCIR links (Fig. 6 (c)). It is also observed that both SNR distributions show a clear west-east asymmetry caused by the sunlight. Therefore, CSCR and SCIR placed close to the window (in the west edge) obtain approximately 4.6 dB and 4 dB less SNR than receivers located in the opposite edge of the room (in the east edge). However, apart from this variation, both SNR figures exhibit very smooth spatial changes. In fact, if the inclination caused by sunlight is neglected, the maximum SNR variation for the CSCR links is of only 5 dB, while the variation for SCIR links is of hardly 0.6 dB. Thus, SCIR links produce more uniform channels in terms of SNR than CSCR links. This intuitive result is due to the higher number of spots employed by SCIR links, as a consequence of the receiver total FOV constraints. Note that, absolute values of SNR are excellent in both figures, higher than 24.6 dB in all receiver positions. On the other hand, and as expected, artificial light from the lamps does not affect the SNR. This is because both receivers are able to avoid these light sources, rejecting all shot noise they induce.
On the contrary, the spatial distribution of the channel BW presents very abrupt variations, as depicted in Fig. 6 (b) and (d). These abrupt variations, of tens of GHz, are due to the changes in the receiver orientation when it moves along the room. However, despite these variations, the obtained BW is always higher than 1 GHz and 1.2 GHz for CSCR links and SCIR links, respectively. Note that, now, the positions with higher BW do not coincide with the coordinates of the transmitter spots. Again, Fig. 6 (b) and (b) show a clear west-east asymmetry of the channel BW due to the higher level of sunlight in the west part of the room caused by the window. However, here the channel BW behavior is different from the SNR behavior and, now, receivers located in the west half of the room obtain better results than receivers located in the east half.
Since SNR and channel BW depend on the receiver position, to compare the performance of the two link configurations, a statistical approach has been applied. Thus, a large number (10^3) of receiver positions have been randomly chosen and the corresponding communications links have been simulated for each in order to obtain statistical results for the system performance. In these new simulations, the power requirements to achieve a bit error rate (BER) not exceeding 10^{-9} and the channel BW have been computed. The BER is given by

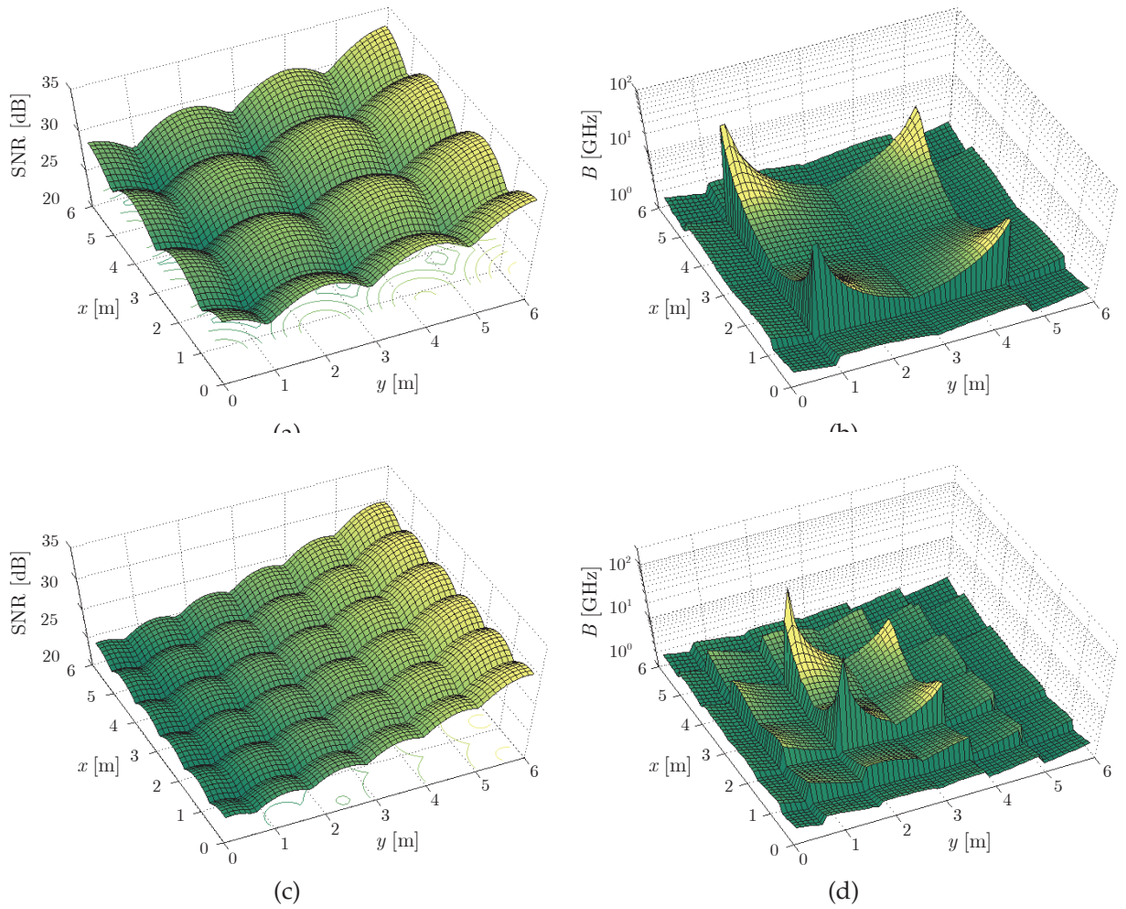

Fig. 6. Signal-to-noise ratio and channel bandwidth spatial distributions for CSCR links and SCIR links. (a) SNR for CSCR links. (b) Channel BW for CSCR links. (c) SNR for SCIR links. (b) Channel BW for SCIR links. CSCR links employ a MBT with 16 beams and a receiver with a $\text{FOV}_{\text{total}} = 45°$. SCIR links uses a MBT with 36 beams and a receiver with a $\text{FOV}_{\text{total}} = 30°$. A transmitter power $P_{tx} = 200$ mW is assumed in all cases.

BER$= Q(\text{SNR})$, so a SNR of 15.6 dB is required to achieve 10^{-9} BER, neglecting the effects of multipath distortion and assuming on-off keying (OOK) modulation (Kahn & Barry, 1997). Fig. 7 (a) presents the average transmitter power to achieve 10^{-9} BER for CSCR links and SCIR links, as a function of the receiver location percentage. In this figure, it is clearly observed that both types of links require very similar transmitter powers. In fact, for 95% location percentage, CSCR links require 17.5 dBm while SCIR links need 17.8 dBm. Thus, CSCR links are lightly superior to SCIR links in terms of power efficiency. This is due to CSCR links divide the same power between fewer beams and, hence, they waste less power illuminating spots different from the selected one. However, when receivers performance is compared in terms of channel BW, the result is just the opposite and, in this case, SCIR links achieve higher BW than CSCR links, as shown in Fig. 7 (b). In particular, for 95% location percentage, the BW of CSCR links is approximately 1.1 GHz, while in SCIR links the BW is better than 1.3 GHz.
The effect of blockage and optical aberrations in system performance has also been analyzed in these links. To emulate signal blockage, the best spot (i.e., the spot which provides the highest

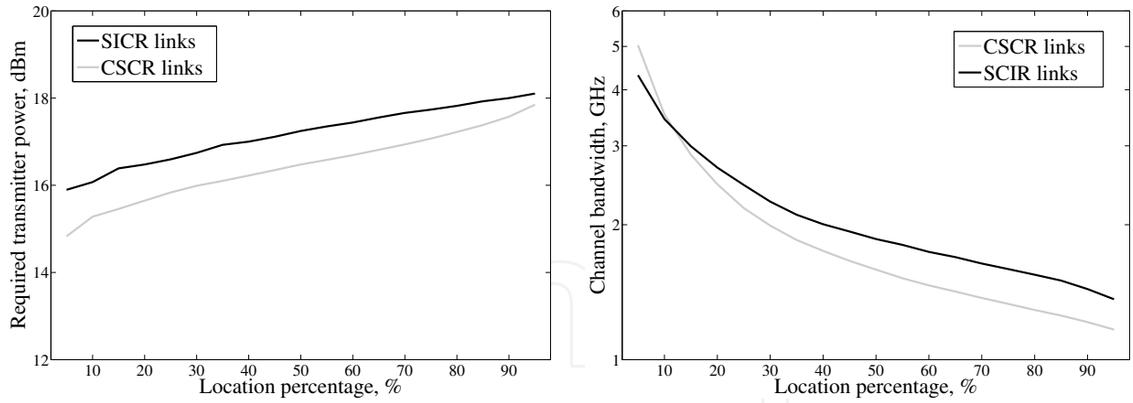

(a) (b)

Fig. 7. (a) Required transmitter power to achieve a BER$< 10^{-9}$ and (b) channel bandwidth as a function of the receiver location percentage.

SNR) within the receivers $\text{FOV}_{\text{total}}$ has been discarded in all links. Thus, since receivers are forced to point at an alternative spot, the transmitter power requirements increase. However, due to the proximity between spots, for 95% location percentage, such an increase is only by 1.6 dB for CSCR links and 0.5 dB for SCIR links. Finally, to include optical aberrations in the simulations, an expansion of the projected spots has been assumed so that for a 10-cm diffusing spot 2 m away from the receiver, the diameter of the image spots varies between 1.52 mm an 2.28 mm, for arrival angles $\psi = 0^\circ$ and $\psi = 30^\circ$, respectively. Thus, since the area of image spots is greater than the photodetector area, part of the received power is lost. In particular, our simulations show that, for 95% location percentage, optical aberrations cause an increase of 0.7 dB in transmitter power requirements.

5. Conclusion

In this chapter, the impact of single-channel receivers on channel properties has been investigated. By numerical simulations, the main performance indicators of two link configurations consisting of a MBT and the proposed CSCR and SCIR have been calculated in a typical indoor environment. The obtained results show the advantages and weaknesses of each receiver structure and have proved the great potential of both SCR when operating in a multispot diffusing configuration. From the analysis of these results, it can be concluded that: (a) both receiver structures obtain excellent results in terms of SNR and channel BW, (b) when reducing transmitter spot size, both SNR and BW are significantly improved at the expense of increasing the search time of the receivers algorithm, (c) as receivers move towards the window sunlight degrades SNR, but channel BW is improved, (d) artificial light does not affect system performance, (e) the joint selection of the receiver total FOV and the number of spots makes CSCR links better than SCIR links in terms of power efficiency and worse in terms of channel BW, and (f) blockage and optical aberrations have a low impact on system performance.

6. Acknowledgment

This work was supported by the Spanish Ministerio de Ciencia e Innovación, Project TEC2008-06598.

7. References

Akavan, K., Kavehrad, M. & Jivkova, S. T. (2002). High-speed power-efficient indoor wireless infrared communication using code combining-Part I, *IEEE Transactions on Communications* 50(7): 1098–1109.

Al-Ghamdi, A. & Elmirghani, J. (2003a). Optimization of a triangular PFDR antenna in a fully diffuse OW system influenced by background noise and multipath propagation, *IEEE Transactions on Communications* 12: 2103–2113.

Al-Ghamdi, A. & Elmirghani, J. (2003b). Performance evaluation of a pyramidal fly-eye diversity antena in an indoor optical wireless multipath propagation environment under very directive noise sources, *IEE Proc-Optoelectron.* 150: 482–489.

Al-Ghamdi, A. & Elmirghani, J. (2004a). Line strip spot-diffusing transmitter configuration for optical wireless systems influenced by background noise and multipath dispersion, *IEEE Transactions on Communications* 52(01): 37–45.

Al-Ghamdi, A. & Elmirghani, J. (2004b). Spot diffusing technique and angle diversity performance for high speed indoor diffuse infra-red wireless transmission, *IEE Proc.-Optoelectron.* 151: 46–52.

Alves, L., Aguiar, R., de Vasconcelos, E. & Cura, J. (2000). A sectored receiver for infrared wireless networks, *IEEE International Symposium on Circuits and Systems*, Geneva, pp. 429–432.

Barry, J. (1994). *Wireless Infrared Communications*, Kluwer Academic Publishers.

Barry, J., Kahn, J., Krause, W. J., Lee, E. A. & Messerschmitt, D. G. (1993). Simulation of multipath impulse response for wireless optical channels, *IEEE Journal on Selected Areas in Communications* 11(3): 367–379.

Bellon, J., Sibley, M., Wisely, D. & Greaves, S. (1999). Hub architecture for infra-red wireless networks in office enviroments, *IEE Proc.-Optoelectron.* 146(2): 78–82.

Boucouvalas, A. (1996). Indoor ambient light noise and its effect on wireless optical links, *IEE Proc.-Optoelectron.* 143: 334–338.

Carruther, J. & Kahn, J. (2000). Angle diversity for nondirected wireless infrared communication, *IEEE Transactions on Communications.* 48(6): 960–969.

Castillo-Vázquez, M., García-Zambrana, A. & Puerta-Notario, A. (2004). Angle diversity with rate-adaptive transmission using repetition coding and variable silence periods for wireless infrared communications, *IEEE 59th Vehicular Technology Conference, VTC '04-Spring*, Vol. 1, pp. 415–419.

Castillo-Vázquez, M. & Puerta-Notario, A. (2005). Single-channel imaging receiver for optical wireless communications, *IEEE Communications Letters* 9(10): 897–899.

Djahani, P. & Kahn, J. (2000). Analysis of infrared wireless links employing multibeam transmitters and imaging diversity receivers, *IEEE Transactions on Communications* 48(12): 2077–2088.

Eardley, P. L., Wisely, D. R., Wood, D. & McKee, P. (1996). Holograms for optical wireless LANs, *IEE Proc.-Optoelectron.* 143(6): 365–369.

Gfeller, F. & Bapst, U. (1979). Wireless in-house data communications via diffuse infrared radiation, *Proceedings of the IEEE* 67: 1474–1486.

Jivkova, S., Hristov, B. & Kavehrad, M. (2004). Power-efficient multispot-diffuse multiple-input-multiple-output approach to broad-band optical wireless communications, *IEEE Transactions on Vehicular Technology* 53(3): 882–889.

Jivkova, S. & Kavehrad, M. (2001). Receiver designs and channel characterization for multi-spot high-bit-rate wireless infrared communications, *IEEE Transactions on Communications* 49(12): 2145–2153.

Jivkova, S. & Kavehrad, M. (2003). Shadowing and blockage in indoor optical wireless communications, *IEEE Global Telecommunications Conference, GLOBECOM '03.*, San Francisco, USA, pp. 3269–3273.

Jivkova, S. & Kavehrad, M. (2005). Transceiver design concept for cellular and multispot diffusing regimes of transmission, *EURASIP Journal on Applied Signal Processing* 1: 30–38.

Jivkova, S. T. & Kavehrad, M. (2000). Multispot diffusing configuration for wireless infrared access, *IEEE Transactions on Communications* 48(6): 970–978.

Jungnickel, V., Forck, A., Haustein, T., Kruger, U., Pohl, V. & von Helmolt, C. (2003). Electronic tracking for wireless infrared communications, *IEEE Transactions on Wireless Communications* 2(5): 989–999.

Kahn, J. & Barry, J. (1997). Wireless infrared communications, *Proceedings of the IEEE* 85(2): 265–298.

Kahn, J. M., Barry, J. R., Audeh, M. D., Carruthers, J. B., Krause, W. J. & Marsh, G. W. (1994). Non-directed infrared links for high-capacity wireless lans, *IEEE Personal Communications* 1(2).

Kahn, J. M., You, R., Djahani, P., A.G.Weisbin, Teik, B. K. & Tang, A. (1998). Imaging diversity receivers for high-speed infrared wireless communications, *IEEE Communications Magazine* 36: 88–94.

Kavehrad, M. & Jivkova, S. (2003). Indoor broadband optical wireless communications: optical subsystems design and their impact on channel characteristics, *Optical Wireless Communications* pp. 30–35.

Moreira, A., Valadas, R. & Duarte, A. O. (1997). Optical interference produced by artificial light, *Wireless Networks* 3(2): 131–140.

Otte, R., de Jong, L. & van Roermund, A. (1999). *Low-Power Wireless Infrared Communications*, Kluwer Academic Publishers.

Pakravan, M. R., Simova, E. & Kavehrad, M. (1996). Holographic diffusers for indoor infrared communication systems, *Proc. 'Communications: The Key to Global Prosperity Global Telecommunications Conf. GLOBECOM '96*, Vol. 3, pp. 1608–1612.

Tang, A., Kahn, J. & Ho, K.-P. (1996). Wireless infrared communication links using multi-beam transmitters and imaging receivers, *IEEE International Conference on Communications, ICC 96, Conference Record, Converging Technologies for Tomorrow's Applications.*, Vol. 1, pp. 180–186vol.1.

Tavares, A., Valadas, R. & de Oliveira Duarte, A. (1995). Performance of an optical sectored receiver for indoor wireless communications systems in presence of artificial and natural noise sources, *SPIE's Photonics East '95 International Symposium*, Philadelphia.

Yun, G. & Kavehrad, M. (1992). Spot-diffusing and fly-eye receivers for indoor infrared wireless communications, *IEEE Conf. on Sel. Topics in Wireless Communications*, Vancouver, Canada, pp. 286–292.

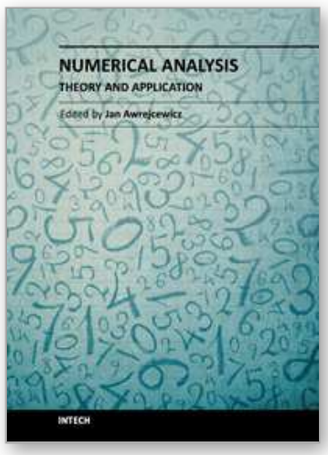

Numerical Analysis - Theory and Application

Edited by Prof. Jan Awrejcewicz

ISBN 978-953-307-389-7
Hard cover, 626 pages
Publisher InTech
Published online 09, September, 2011
Published in print edition September, 2011

Numerical Analysis â€“ Theory and Application is an edited book divided into two parts: Part I devoted to Theory, and Part II dealing with Application. The presented book is focused on introducing theoretical approaches of numerical analysis as well as applications of various numerical methods to either study or solving numerous theoretical and engineering problems. Since a large number of pure theoretical research is proposed as well as a large amount of applications oriented numerical simulation results are given, the book can be useful for both theoretical and applied research aimed on numerical simulations. In addition, in many cases the presented approaches can be applied directly either by theoreticians or engineers.

How to reference

In order to correctly reference this scholarly work, feel free to copy and paste the following:

M. Castillo-Vázquez, A. Jurado-Navas, J.M. Garrido-Balsells and A. Puerta-Notario (2011). Performance Evaluation of Single-Channel Receivers for Wireless Optical Communications by Numerical Simulations, Numerical Analysis - Theory and Application, Prof. Jan Awrejcewicz (Ed.), ISBN: 978-953-307-389-7, InTech, Available from: http://www.intechopen.com/books/numerical-analysis-theory-and-application/performance-evaluation-of-single-channel-receivers-for-wireless-optical-communications-by-numerical-

INTECH
open science | open minds

InTech Europe
University Campus STeP Ri
Slavka Krautzeka 83/A
51000 Rijeka, Croatia
Phone: +385 (51) 770 447
Fax: +385 (51) 686 166
www.intechopen.com

InTech China
Unit 405, Office Block, Hotel Equatorial Shanghai
No.65, Yan An Road (West), Shanghai, 200040, China
中国上海市延安西路65号上海国际贵都大饭店办公楼405单元
Phone: +86-21-62489820
Fax: +86-21-62489821

IntechOpen